


Atomically thin metallic Si and Ge allotropes with high Fermi velocitiesChin-En Hsu ¹, Yung-Ting Lee ², Chieh-Chun Wang ¹, Chang-Yu Lin,¹ Yukiko Yamada-Takamura,³ Taisuke Ozaki,⁴ and Chi-Cheng Lee ^{1,5,*}¹*Department of Physics, Tamkang University, Tamsui, New Taipei 251301, Taiwan*²*Department of Electrophysics, National Yang Ming Chiao Tung University, Hsinchu 300093, Taiwan*³*School of Materials Science, Japan Advanced Institute of Science and Technology (JAIST), 1-1 Asahidai, Nomi, Ishikawa 923-1292, Japan*⁴*Institute for Solid State Physics, The University of Tokyo, 5-1-5 Kashiwanoha, Kashiwa, Chiba 277-8581, Japan*⁵*Research Center for X-ray Science, College of Science, Tamkang University, Tamsui, New Taipei 251301, Taiwan* (Received 24 July 2022; revised 9 January 2023; accepted 24 February 2023; published 9 March 2023)

Silicon and germanium are well-known materials used to manufacture electronic devices for integrated circuits, but they themselves are not considered as promising options for interconnecting the devices due to their semiconducting nature. We have discovered that both Si and Ge atoms can form unexpected metallic monolayer structures with a square lattice which are more stable than the semimetallic silicene and germanene, respectively, in line with the energetically more favored dumbbell and wavy-bilayer structures. More importantly, these two-dimensional allotropes of Si and Ge host Dirac fermions with Fermi velocities superior to those in graphene, indicating that the metal wires needed in the silicon-based integrated circuits can be made of the Si atom itself without incompatibility, allowing for all-silicon-based integrated circuits.

DOI: [10.1103/PhysRevB.107.115410](https://doi.org/10.1103/PhysRevB.107.115410)**I. INTRODUCTION**

Ever since graphene was discovered [1], the physical properties of two-dimensional (2D) materials have been extensively explored for realizing higher-performance electronic devices used in modern technology [2,3]. Heterostructures with diverse electronic structures can be further built in a manner similar to playing with Lego blocks by stacking layered materials with different twisted angles [4,5]. Among the known 2D materials, silicene and germanene, the well-known thinnest Si and Ge allotropes, respectively, are of great interest owing to their hexagonal structures that can host Dirac fermions, akin to graphene [6,7]. Another fact is that the hexagonal structure forms the “Lego” layer for building the 3D diamond structure along the (111) direction, which gives the silicon and germanium used in the semiconductor industry. A metallic silicene-based layer useful for devices has also been experimentally demonstrated [8].

The miniaturization of integrated circuits requires not only high-performance transistors but also highly efficient interconnects to keep up with Moore’s law [9,10]. Due to the semiconducting nature, Si and Ge allotropes have not generally been considered as a good option for connecting the miniaturized silicon-based transistors. Instead, the interconnecting wires are usually made of metals such as copper; however, the diffusion of copper into semiconducting materials could severely affect the designed doping effects [11,12]. Other metals might possess insufficient conductivity or lack availability for manufacturing. For ultimate miniaturization, it

is desirable to have an atomic-scale interconnect made of the Si atom itself with high electrical conductivity, allowing for all-Si-based integrated circuits.

Several interesting 2D Si and Ge allotropes have been found to possess lower energies than silicene and germanene, respectively, such as those crystallized in the so-called “MoS₂” [13], dumbbell [14–16], and wavy-bilayer (w-BL) [17] structures, showing the possible existence of an energetically competitive Si or Ge allotrope with the aforementioned metallic property. Along this line, we have discovered atomically thin metallic layers composed of Si and Ge atoms with Fermi velocities higher than those of the Dirac fermions in graphene from first-principles calculations, and they are also energetically more stable than silicene and germanene, respectively, in line with the energetically more favored dumbbell and w-BL structures.

To introduce the physical properties of the Si and Ge layers, we will first discuss how to extract the monolayer structure from the diamond structure. The total energies of these monolayers in comparison with several selected Si and Ge allotropes and phonon dispersions will then be presented to address their structural stability. Subsequently, the electronic structures, especially the metallic behavior with high Fermi velocities, will be discussed. The paper is organized as follows. The geometrical structure is described in Sec. II. The computational detail of the first-principles calculations that lead us to find the structures is given in Sec. III. The relative energies and phonon instability are addressed in Sec. IV. The band structures, density of states, and Fermi velocities are presented in Sec. V, followed by the discussion of bonding nature through the charge density distribution in Sec. VI. Finally, the energy gain in the bilayer case and a conclusion are given in Secs. VII and VIII, respectively.

*cclee@mail.tku.edu.tw

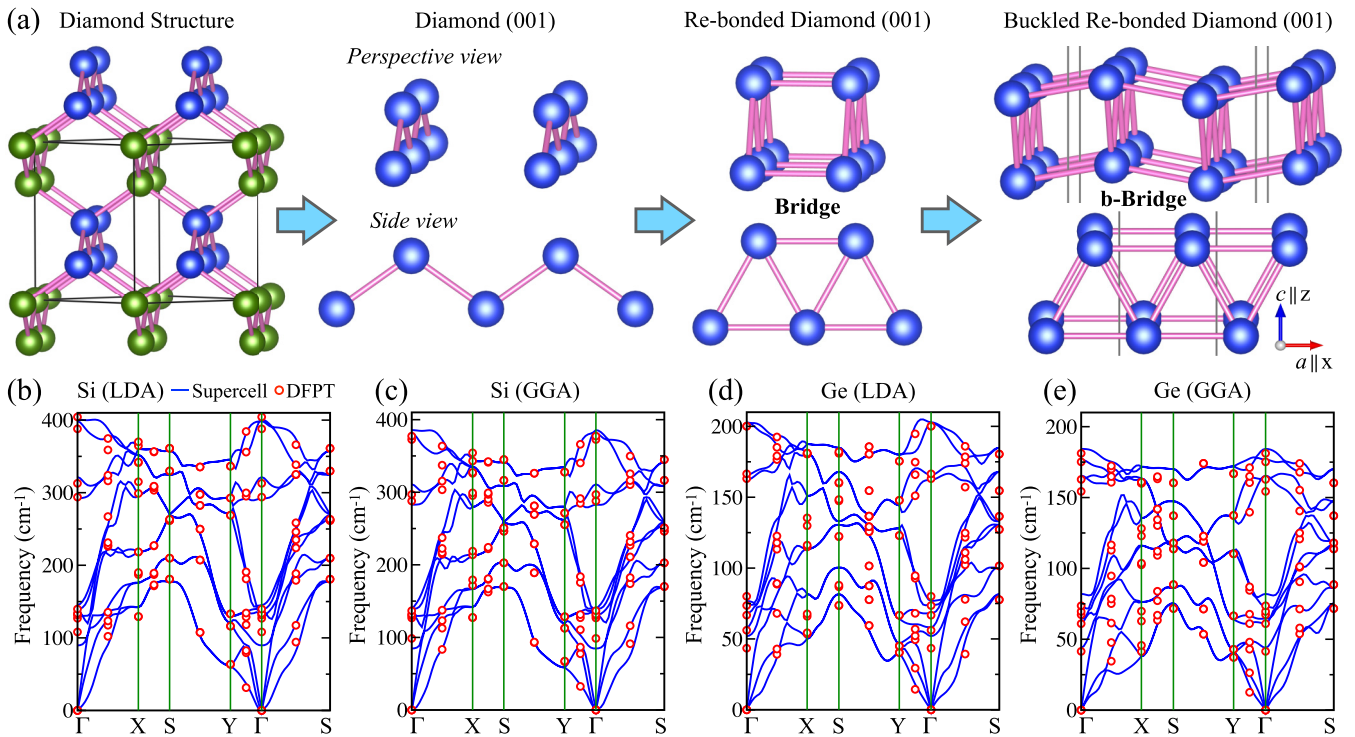


FIG. 1. (a) Schematics of the formation of bridge and b-bridge structures from the diamond structure. Phonon dispersion of Si b-bridge within (b) LDA and (c) GGA. Phonon dispersion of Ge b-bridge within (d) LDA and (e) GGA. Γ , X, S, and Y denote (0, 0), (0.5, 0), (0.5, 0.5), and (0, 0.5) in units of the reciprocal lattice vectors. The curves are obtained from the supercell force-constant calculations using OPENMX code, and the circles denote the result of density functional perturbation theory (DFPT) using QUANTUM ESPRESSO code. The structures shown in (a) are generated using VESTA software [18].

II. GEOMETRICAL STRUCTURE

The formation of the atomically thin layer is presented in Fig. 1(a). The strategy for finding this structure is to reduce the thickness of the diamond structure along the [001] direction and study underexplored 2D structures having a square lattice. Note that the direction is aligned with the Si(001) substrate surface normal, which is commonly adopted for fabricating a variety of devices. As shown in Fig. 1(a), the 1D buckling chain, like the polyacetylene described by the Su-Schrieffer-Heeger (SSH) model [19], can be extracted from the (001) surface. After introducing new bonding between the chains, a bridgelike structure, which will be dubbed “bridge,” is formed. By further introducing interchain buckling in the bridge structure, the buckled re-bonded diamond (001) layer is revealed, and this structure will be dubbed “b-bridge.”

To demonstrate that b-bridge is energetically competitive and dynamically stable, we have calculated the total energy and phonon dispersion using the OPENMX code [20] by adopting two sophisticated approximations within the density functional theory [21], the local density approximation (LDA) and the generalized gradient approximation (GGA) [22,23]. To confirm the stability, we have also performed the calculations using another first-principles package, QUANTUM ESPRESSO [24,25], and arrived at the same conclusion. The lattice parameters obtained from both the OPENMX and QUANTUM ESPRESSO codes are listed in the Supplemental Material [26]. The computational details are provided in the next section.

III. COMPUTATIONAL DETAIL

In the calculations using the OPENMX code, norm-conserving pseudopotentials and optimized pseudoatomic basis functions were adopted. Two optimized radial functions were allocated for the s orbital, two were allocated for the p orbital, and one was allocated for the d orbital, for each atom with a cutoff radius of 7 bohrs (C7.0- $s2p2d1$, Si7.0- $s2p2d1$, and Ge7.0- $s2p2d1$). A cutoff energy of 1000 Ry was used for numerical integrations and for the solution of the Poisson equation. For the hexagonal lattice, such as graphene and such as silicene with low buckling, a $60 \times 60 \times 1$ k -point sampling was adopted. For the orthorhombic lattice, for example, the Si b-bridge structure, a $40 \times 20 \times 1$ k -point sampling was used. For the dumbbell structure, a $16 \times 16 \times 1$ k -point sampling was chosen. For the w-BL and AA-stacking bridge (AA-bridge) bilayer structures, $15 \times 30 \times 1$ and $40 \times 40 \times 1$ k -point samplings were adopted. A $20 \times 20 \times 20$ k -point sampling was used for the conventional unit cell of the diamond structure. An electronic temperature of 300 K was chosen for the smearing in the self-consistent calculations. All the lattice parameters listed in the Supplemental Material [26] using the OPENMX code were fully relaxed without considering spin-orbit coupling until the forces and stresses were smaller than 0.0001 hartrees/bohr and 0.03 GPa, respectively. All the slab structures were optimized with the c axis being fixed at 40 Å to ensure that the structures were separated by a thick vacuum layer.

For the phonon calculation of the b-bridge structure, the dynamical matrix was constructed via the real-space force constants collected from the $(10 \times 5 \times 1)$ supercell calculations with the atomic displacement of 0.01 Å. For the phonon calculation of the AA-bridge structure, the dynamical matrix was constructed via the real-space force constants collected from the $(8 \times 8 \times 1)$ supercell calculations with a dense k -point sampling ($8 \times 8 \times 1$ k grids), and the atomic displacement was set to 0.1 Å.

In the calculations using the QUANTUM ESPRESSO code, plane waves were adopted as the basis. The ultrasoft pseudopotentials were chosen to calculate the total energy, band structure, and phonon dispersion without considering spin-orbit coupling. The plane-wave cutoff energy was set to 90 Ry for expanding the wave function, and 720 Ry was set for describing the charge density distribution. For the monolayer systems, $30 \times 30 \times 1$ and $40 \times 20 \times 1$ k -point samplings were adopted for the hexagonal and orthorhombic lattices, respectively. For the dumbbell structure, a $16 \times 16 \times 1$ k -point sampling was used. For the w-BL and AA-bridge structures, $15 \times 30 \times 1$ and $40 \times 40 \times 1$ k -point samplings were adopted. A $20 \times 20 \times 20$ k -point sampling was used for the conventional unit cell of the diamond structure. All the slab structures were optimized with the c axis being fixed at 40 Å to ensure that the structures were separated by a thick vacuum layer. The force of each atom was smaller than 0.001 hartrees/bohr, and the stress threshold was set to 0.5 kbar. The band structures using the hybrid Heyd-Scuseria-Ernzerhof exchange-correlation functional, HSE06 [27], were calculated with $10 \times 5 \times 1$ q grids for the b-bridge structures and $10 \times 10 \times 1$ q grids for graphene, where the structures were obtained from the GGA result. The WANNIER90 code was used to interpolate the HSE06 band structures [28]. The phonon dispersion was calculated via the density functional perturbation theory (DFPT) approach to allow for delivering phonon frequencies at the specified q points without interpolation.

IV. STRUCTURAL STABILITY

The total energies and phonon dispersions of Si b-bridge and Ge b-bridge will be discussed here. As listed in Table I, the Si allotrope in the bridge structure already possesses lower total energy than silicene with low or high buckling, and the Ge allotrope in the bridge structure already possesses lower total energy than germanene with low or high buckling. After introducing the interchain buckling, the total energies of Si b-bridge and Ge b-bridge can be further lowered and become comparable to those of the “MoS₂” dumbbell, and w-BL structures. Note that there exist several different dumbbell structures, and their relative energies can be found elsewhere [16]. In contrast, the total energy becomes higher in the case of C b-bridge, where no interchain buckling can be identified; that is, C b-bridge may be reduced to bridge structure. This is consistent with the fact that puckered structures are preferred by Si and Ge atoms, allowing for diverse forms of bonding [13,29].

Although Si b-bridge and Ge b-bridge are energetically competitive, the b-bridge structure might not be dynamically stable. Recall that silicene with high buckling and germanene

TABLE I. Total energies of the studied structures with high buckling (HB), bridge structures, b-bridge structures, “MoS₂” structures, dumbbell structures, w-BL structures, and diamond structures composed of C, Si, and Ge atoms relative to those of graphene, silicene with low buckling (LB silicene), and LB germanene, respectively.

Element	Structure	Total energy (eV/atom)			
		OPENMX		QE*	
		LDA	GGA	LDA	GGA
C	Graphene	0	0	0	0
	Bridge or b-bridge	1.700	1.769	1.731	1.786
	Diamond	-0.085	0.100	-0.037	0.137
Si	LB silicene	0	0	0	0
	HB silicene	-0.018	0.102	-0.044	0.066
	“MoS ₂ ”	-0.095	-0.031	-0.078	-0.016
	Bridge	-0.235	-0.119	-0.227	-0.114
	b-Bridge	-0.243	-0.127	-0.240	-0.127
	Dumbbell	-0.250	-0.222	-0.230	-0.204
	w-BL	-0.318	-0.257	-0.292	-0.231
	Diamond	-0.812	-0.698	-0.755	-0.641
Ge	LB germanene	0	0	0	0
	HB germanene	-0.204	-0.127	-0.146	-0.075
	“MoS ₂ ”	-0.193	-0.141	-0.158	-0.115
	Bridge	-0.251	-0.148	-0.195	-0.099
	b-Bridge	-0.273	-0.176	-0.216	-0.125
	Dumbbell	-0.210	-0.175	-0.200	-0.169
	w-BL	-0.281	-0.211	-0.249	-0.181
	Diamond	-0.674	-0.538	-0.621	-0.484

*QE, QUANTUM ESPRESSO.

with high buckling also possess lower total energies than their forms with low buckling but they are in fact not stable due to the presence of imaginary-frequency vibrational modes [6]. To demonstrate the dynamical stability of Si b-bridge and Ge b-bridge, their phonon dispersions within both LDA and GGA are presented in Figs. 1(b)–1(e). Overall, the frequencies in Ge b-bridge are lower than those in Si b-bridge due to the heavier mass of the Ge atom, and the LDA calculations give higher frequencies than the GGA ones due to the delivered shorter lattice constants that may lead to overbinding. The absence of imaginary frequencies in all the dispersions advocates for the dynamical stability of Si b-bridge and Ge b-bridge.

V. ELECTRONIC STRUCTURE

The electronic band structures and density of states shown in Figs. 2(a)–2(d) indicate that both Si b-bridge and Ge b-bridge are metallic, similar to the case of 2D metallic borophene in contrast to the semiconducting bulk boron allotropes [30]. Note that a high Fermi velocity of 1.09×10^6 m/s can be identified within GGA after arranging borophene on the Al(111) surface [31]. The electronic velocities obtained from the calculated momentum matrix elements [32], which are also reflected by the slopes in the band dispersion, are presented in Figs. 2(e) and 2(f). Like the metals that are proposed to replace copper for the interconnects [33], the electronic velocities in Si b-bridge and Ge b-bridge reach the order of 10^6 m/s. The high velocities can be visualized from

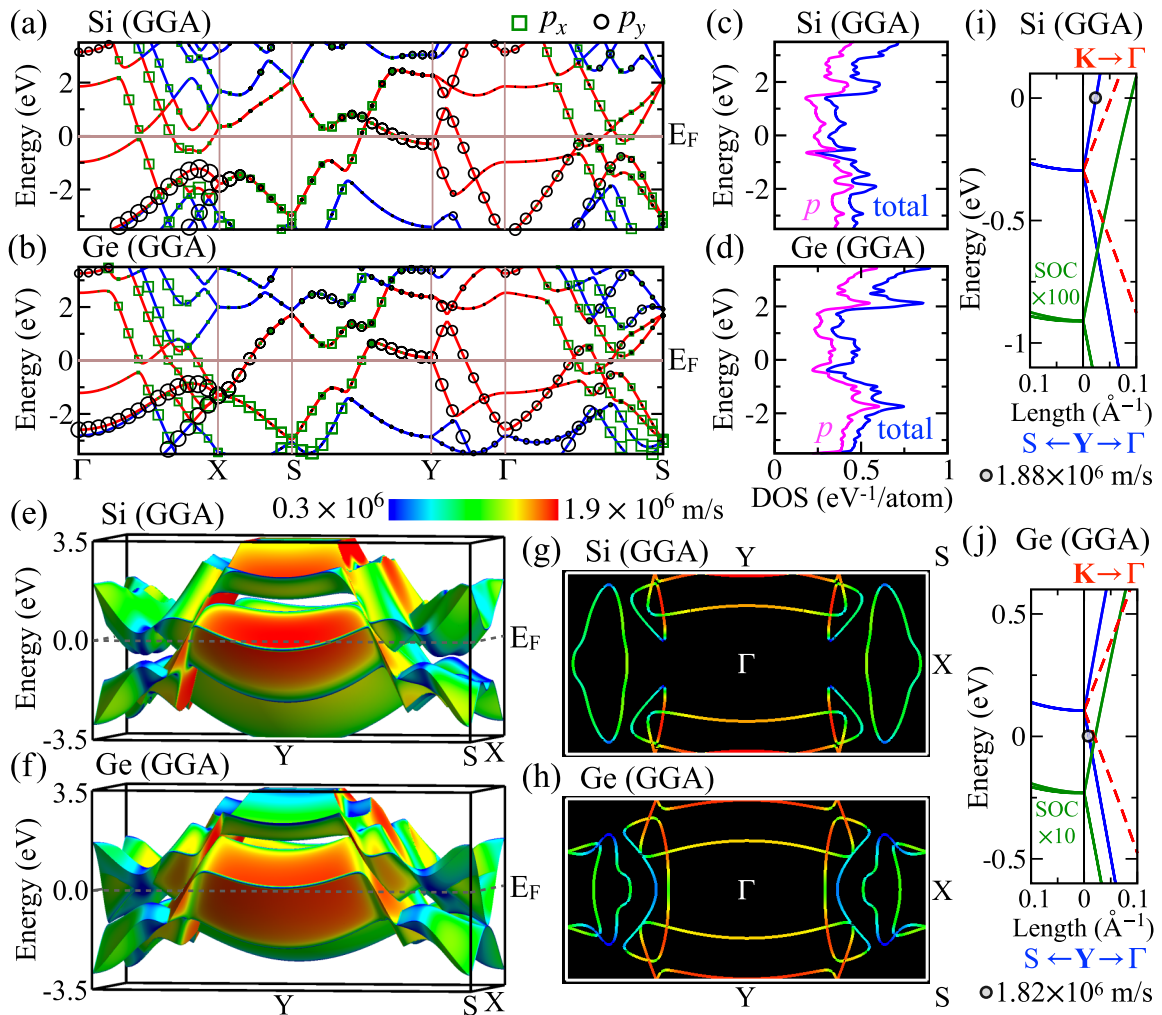


FIG. 2. Band structures of (a) Si b-bridge and (b) Ge b-bridge within GGA using OPENMX code. Density of states (DOS) with the p -orbital contribution of (c) Si b-bridge and (d) Ge b-bridge. The red bands in (a) and (b) are colored with the magnitudes of velocities (red, high; blue, low) for (e) Si b-bridge and (f) Ge b-bridge. E_F denotes the Fermi level. Fermi surfaces of (g) Si b-bridge and (h) Ge b-bridge. After taking spin-orbit coupling into account, the Dirac cone in graphene (red dashed curves) is aligned to the Dirac cones in (i) Si b-bridge and (j) Ge b-bridge (blue curves). The bands with the strength of spin-orbit coupling enlarged by (i) 100 times and (j) 10 times are presented by green curves. The velocities at the Fermi levels as marked by the circles in (i) and (j) are provided. The plots in (e)–(h) are generated using FERMISURFER software. The LDA result and the band structures obtained using QUANTUM ESPRESSO code are shown in the Supplemental Material [26].

the pyramids shown in Figs. 2(e) and 2(f) with steep slopes in both x and y directions.

In Figs. 2(g) and 2(h), the Fermi surfaces generated using FERMISURFER software [34] are presented, and the highest Fermi velocities are both found at Y in the 2D Brillouin zone. The magnitudes of the velocities at Y reach 1.88×10^6 (1.89×10^6) and 1.82×10^6 (1.89×10^6) m/s in Si b-bridge and Ge b-bridge, respectively, within GGA (LDA). Graphene hosts Dirac fermions with the Fermi velocity around 0.9×10^6 m/s within LDA [35,36]. As shown in Figs. 2(i) and 2(j), the magnitudes of the velocities along the Y -to- Γ direction in both the Si b-bridge and Ge b-bridge cases are prominently higher than those along the K -to- Γ direction in graphene within either LDA or GGA. The superior Fermi velocities can also be identified using the HSE06 hybrid functional implemented by the QUANTUM ESPRESSO and WANNIER90 codes (see Supple-

mental Material [26]). Since Fermi velocities in 2D materials can be modified by introducing a substrate [31,35] and many-body interactions beyond LDA or GGA [36,37], the Fermi velocities could be higher, for example, 2.48×10^6 m/s in Si b-bridge and 2.44×10^6 m/s in Ge b-bridge at the HSE06 level [26].

The bands near the Fermi level at Y exhibit an interesting feature. While one-dimensional Dirac fermions with remarkably high velocities are revealed along the y direction, the bands along the perpendicular direction are relatively flat and form a fourfold-degenerate nodal line, as shown in Figs. 2(e) and 2(f). After taking spin-orbit coupling into account, the nodal line is split into two twofold-degenerate nodal lines, as shown in Figs. 2(i) and 2(j). However, the fourfold degeneracy at Y is intact, forming a Dirac point. The Dirac point at Y , one of the time-reversal-invariant momenta, is protected by

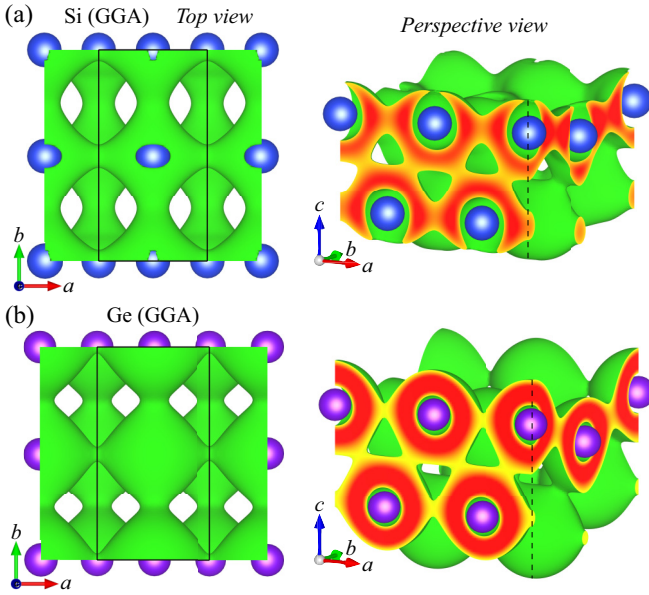


FIG. 3. Top view and perspective view of the isosurface of charge density at (a) 0.052 electrons/bohr³ in Si b-bridge and (b) 0.035 electrons/bohr³ in Ge b-bridge within GGA calculated using OPENMX code. The result within LDA is presented in the Supplemental Material [26].

both time-reversal symmetry and inversion symmetry. The degeneracy is highly tunable, for example, through breaking the inversion symmetry with adatoms.

VI. CHARGE DENSITY DISTRIBUTION

Si and Ge atoms crystallizing in the b-bridge structure with high stability is actually unexpected. Each Si or Ge atom has to accommodate its two s -orbital and two p -orbital electrons to six anisotropic bonds surrounding the atomic center. Consequently, strong covalent bonds such as the fully filled σ and π bonds in silicene and germanene cannot be formed, and the metallicity with partially filled p orbitals is anticipated. As shown in Figs. 2(a) and 2(b), the high velocities along the x and y directions near the Fermi level are contributed from the p_x and p_y orbitals, respectively. By considering that the b-bridge layer is composed of two buckled rectangular-lattice layers, the steep slopes can be attributed to the strong intralayer p_x - p_x and p_y - p_y hopping strengths. The charge density distribution presented in Fig. 3, which is generated using VESTA software, further reveals that the occupied orbitals form a close-packed structure in the ac plane, as a result of rehybridization of s , p_x , and p_z orbitals. On the other hand, electrons distribute more along the y direction in the buckled rectangular-lattice layer, suggesting that the bonds formed by the p_y orbitals are closer to covalent bonding.

VII. AA-STACKING BILAYER STRUCTURE

Here, we will address the energy gain via the interaction between two bridge layers. According to our first-principles calculations, the buckling in both Si b-bridge and Ge b-bridge is suppressed in the formation of the AA-stacking bilayer structure, dubbed “AA-bridge,” in which additional energy

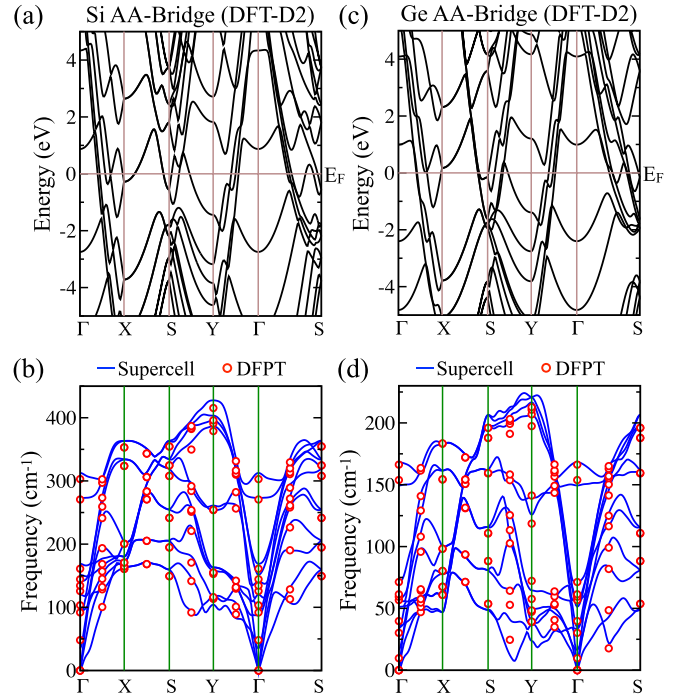


FIG. 4. (a) Band structure and (b) phonon dispersion of Si AA-bridge within DFT-D2 using OPENMX code. The result for Ge AA-bridge is shown in (c) and (d). Phonon frequencies obtained from DFPT calculations using QUANTUM ESPRESSO code are denoted by circles. A similar result obtained from LDA is presented in the Supplemental Material [26].

can be gained via the interlayer interaction. For example, the energies of Si AA-bridge become 225 (382) and 218 (375) meV/atom lower than those of silicene with low buckling, and the energies of Ge AA-bridge become 230 (377) and 165 (305) meV/atom lower than those of germanene with low buckling within GGA (LDA) obtained from the OPENMX and QUANTUM ESPRESSO codes, respectively. By considering the corrected GGA with the van der Waals interactions (density functional theory dispersion correction DFT-D2) [38], the aforementioned energy gains become 348 and 343 meV/atom for Si AA-bridge and 399 and 337 meV/atom for Ge AA-bridge obtained from the OPENMX and QUANTUM ESPRESSO codes, respectively. The lattice parameters of AA-bridge structures are listed in the Supplemental Material [26]. The band structures of Si AA-bridge and Ge AA-bridge are presented in Figs. 4(a) and 4(c), respectively. The steep slopes demonstrate the preservation of the metallic behavior with high Fermi velocities in the formation of the bilayer structures. The phonon dispersions of Si AA-bridge and Ge AA-bridge have been examined within LDA and DFT-D2. The DFT-D2 dispersions are shown in Figs. 4(b) and 4(d), respectively. The resulting absence of imaginary-frequency modes supports the idea that both Si AA-bridge and Ge AA-bridge are dynamically stable.

VIII. CONCLUSION

In conclusion, the bridge-derived structures have demonstrated again that the bonding in the Si and Ge allotropes is

quite flexible, and more low-dimensional Si and Ge structures with multiple buckling forms are expected to possess competitive or even lower energies than the identified allotropes, especially given that the diamond structure sets the lowest-energy limit among the “Lego blocks” (see Table I). The discovery of atomically thin metallic Si b-bridge and Ge b-bridge with the Fermi velocities higher than those of the Dirac fermions in graphene also advocates for the possibility of fabricating all-Si-based electronic devices that can be used in the semiconductor industry, ranging from transistors to interconnects. The buckling form, thickness, orientation, and doped elements all play key roles in the miniature technology. These findings motivate more studies on the Si and Ge phases in between 2D bridge-derived and 3D diamond

structures under various conditions, such as uniaxial strain and/or temperature.

ACKNOWLEDGMENTS

The calculations were carried out using the facilities in JAIST and Tamkang University. C.-C.L. acknowledges the National Science and Technology Council (NSTC) of Taiwan for financial support under Contract No. 110-2112-M-032-016-MY2. Y.-T.L. acknowledges the National Science and Technology Council (NSTC) of Taiwan for financial support under Contract No. 111-2811-M-A49-507. Y.Y.-T. acknowledges support from JSPS KAKENHI Grants No. JP21H05232 and No. JP21H05236.

- [1] A. K. Geim and K. S. Novoselov, *Nat. Mater.* **6**, 183 (2007).
- [2] G. Fiori, F. Bonaccorso, G. Iannaccone, T. Palacios, D. Neumaier, A. Seabaugh, S. K. Banerjee, and L. Colombo, *Nat. Nanotechnol.* **9**, 768 (2014).
- [3] M. C. Lemme, D. Akinwande, C. Huyghebaert, and C. Stampfer, *Nat. Commun.* **13**, 1392 (2022).
- [4] A. K. Geim and I. V. Grigorieva, *Nature (London)* **499**, 419 (2013).
- [5] R. Ribeiro-Palau, C. Zhang, K. Watanabe, T. Taniguchi, J. Hone, and C. R. Dean, *Science* **361**, 690 (2018).
- [6] S. Cahangirov, M. Topsakal, E. Aktürk, H. Şahin, and S. Ciraci, *Phys. Rev. Lett.* **102**, 236804 (2009).
- [7] S. Balendhran, S. Walia, H. Nili, S. Sriram, and M. Bhaskaran, *Small* **11**, 640 (2015).
- [8] T. G. Gill, A. Fleurence, B. Warner, H. Prüser, R. Friedlein, J. T. Sadowski, C. F. Hirjibehedin, and Y. Yamada-Takamura, *2D Mater.* **4**, 021015 (2017).
- [9] M. R. Baklanov, C. Adelman, L. Zhao, and S. D. Gendt, *ECS J. Solid State Sci. Technol.* **4**, Y1 (2014).
- [10] S. Liu, K. Sweatman, S. McDonald, and K. Nogita, *Materials* **11**, 1384 (2018).
- [11] C.-K. Hu and J. Harper, *Mater. Chem. Phys.* **52**, 5 (1998).
- [12] J. Harper, E. Colgan, C.-K. Hu, P. Hummel, L. Buchwalter, and C. Uzoh, *MRS Bull.* **19**, 23 (1994).
- [13] F. Gimbert, C.-C. Lee, R. Friedlein, A. Fleurence, Y. Yamada-Takamura, and T. Ozaki, *Phys. Rev. B* **90**, 165423 (2014).
- [14] V. O. Özçelik, H. H. Gurel, and S. Ciraci, *Phys. Rev. B* **88**, 045440 (2013).
- [15] T. Leoni, C. Hogan, K. Zhang, M. Daher Mansour, R. Bernard, R. Parret, A. Resta, S. Colonna, Y. Borensztein, F. Ronci, G. Prévot, and L. Masson, *J. Phys. Chem. C* **125**, 17906 (2021).
- [16] P. Borlido, C. Rödl, M. A. L. Marques, and S. Botti, *2D Mater.* **5**, 035010 (2018).
- [17] R. Yaokawa, T. Ohsuna, T. Morishita, Y. Hayasaka, M. J. S. Spencer, and H. Nakano, *Nat. Commun.* **7**, 10657 (2016).
- [18] K. Momma and F. Izumi, *J. Appl. Cryst.* **44**, 1272 (2011).
- [19] W. P. Su, J. R. Schrieffer, and A. J. Heeger, *Phys. Rev. Lett.* **42**, 1698 (1979).
- [20] T. Ozaki, *Phys. Rev. B* **67**, 155108 (2003).
- [21] W. Kohn and L. J. Sham, *Phys. Rev.* **140**, A1133 (1965).
- [22] D. M. Ceperley and B. J. Alder, *Phys. Rev. Lett.* **45**, 566 (1980).
- [23] J. P. Perdew, K. Burke, and M. Ernzerhof, *Phys. Rev. Lett.* **77**, 3865 (1996).
- [24] P. Giannozzi, S. Baroni, N. Bonini, M. Calandra, R. Car, C. Cavazzoni, D. Ceresoli, G. L. Chiarotti, M. Cococcioni, I. Dabo, A. D. Corso, S. de Gironcoli, S. Fabris, G. Fratesi, R. Gebauer, U. Gerstmann, C. Gougoussis, A. Kokalj, M. Lazzeri, L. Martin-Samos, N. Marzari *et al.*, *J. Phys.: Condens. Matter* **21**, 395502 (2009).
- [25] P. Giannozzi, O. Andreussi, T. Brumme, O. Bunau, M. B. Nardelli, M. Calandra, R. Car, C. Cavazzoni, D. Ceresoli, M. Cococcioni, N. Colonna, I. Carnimeo, A. D. Corso, S. de Gironcoli, P. Delugas, R. A. DiStasio, A. Ferretti, A. Floris, G. Fratesi, G. Fugallo *et al.*, *J. Phys.: Condens. Matter* **29**, 465901 (2017).
- [26] See Supplemental Material at <http://link.aps.org/supplemental/10.1103/PhysRevB.107.115410> for the lattice parameters together with the supplemental electronic band structures, charge density isosurfaces, and phonon dispersion.
- [27] J. Heyd, G. E. Scuseria, and M. Ernzerhof, *J. Chem. Phys.* **124**, 219906 (2006).
- [28] G. Pizzi, V. Vitale, R. Arita, S. Blügel, F. Freimuth, G. Géranton, M. Gibertini, D. Gresch, C. Johnson, T. Koretsune, J. Ibañez-Azpiroz, H. Lee, J.-M. Lihm, D. Marchand, A. Marrazzo, Y. Mokrousov, J. I. Mustafa, Y. Nohara, Y. Nomura, L. Paulatto *et al.*, *J. Phys.: Condens. Matter* **32**, 165902 (2020).
- [29] H. Şahin, S. Cahangirov, M. Topsakal, E. Bekaroglu, E. Akturk, R. T. Senger, and S. Ciraci, *Phys. Rev. B* **80**, 155453 (2009).
- [30] A. J. Mannix, X.-F. Zhou, B. Kiraly, J. D. Wood, D. Alducin, B. D. Myers, X. Liu, B. L. Fisher, U. Santiago, J. R. Guest, M. J. Yacaman, A. Ponce, A. R. Oganov, M. C. Hersam, and N. P. Guisinger, *Science* **350**, 1513 (2015).
- [31] Y. Jiao, F. Ma, X. Zhang, and T. Heine, *Chem. Sci.* **13**, 1016 (2022).
- [32] C.-C. Lee, Y.-T. Lee, M. Fukuda, and T. Ozaki, *Phys. Rev. B* **98**, 115115 (2018).
- [33] D. Gall, *J. Appl. Phys.* **119**, 085101 (2016).
- [34] M. Kawamura, *Comput. Phys. Commun.* **239**, 197 (2019).
- [35] C. Hwang, D. A. Siegel, S.-K. Mo, W. Regan, A. Ismach, Y. Zhang, A. Zettl, and A. Lanzara, *Sci. Rep.* **2**, 590 (2012).
- [36] P. E. Trevisanutto, C. Giorgetti, L. Reining, M. Ladisa, and V. Olevano, *Phys. Rev. Lett.* **101**, 226405 (2008).
- [37] D. C. Elias, R. V. Gorbachev, A. S. Mayorov, S. V. Morozov, A. A. Zhukov, P. Blake, L. A. Ponomarenko, I. V. Grigorieva, K. S. Novoselov, F. Guinea, and A. K. Geim, *Nat. Phys.* **7**, 701 (2011).
- [38] S. Grimme, *J. Comput. Chem.* **27**, 1787 (2006).